H1-prelim-02-015
April 2002

Elastic electroproduction of ρ mesons with $8 < Q^2 < 60\ \mathrm{GeV}^2$ at HERA

H1 Collaboration

Abstract

Elastic electroproduction of rho mesons is studied at HERA with the H1 detector using an integrated luminosity of 42.4 pb^{-1} in the kinematic range $8 < Q^2 < 60$ GeV^2, $40 < W < 180$ GeV, $0 < |t| < 0.5$ GeV^2. The increase of luminosity compared to previous measurments gives access to the Q^2 domain where perturbative QCD is expected to apply. Cross sections have been measured as a function of Q^2, W and t . The W dependence of the $\gamma^* p$ cross section is observed to increase with Q^2 from values compatible with a soft Pomeron exchange at low Q^2 to hard dependence at large Q^2. Spin density matrix elements are measured and their dependence is compared with a 2 gluon exchange model.

1 Introduction

The subject of this paper is the study of the elastic electroproduction of ρ mesons in ep scattering at high energy:

$$e + p \rightarrow e + \rho \; + p; \quad \rho \rightarrow \pi^+\pi^-. \tag{1}$$

The scattered proton can also be excited into a system Y of mass M_Y which is much lower than the photon–proton centre of mass energy W ("proton dissociative" scattering).

The kinematic domain of the measurement is:

$$\begin{aligned} 8 < \; & Q^2 & < 60 \text{ GeV}^2 \\ 40 < \; & W & < 180 \text{ GeV} \\ 0 < \; & |t| & < 0.5 \text{GeV}^2. \end{aligned} \tag{2}$$

Three angles are defined to characterise the electroproduction of vector mesons decaying into two charged particles: Φ is the angle between the VM production plane (defined as the plane containing the virtual photon and the VM directions) and the electron scattering plane in the $(\gamma^\star p)$ centre of mass system, θ^* and ϕ are the polar and the azimuthal angles, respectively, of the positively charged decay particle in the VM rest frame the quantisation axis being taken as the direction opposite to that of the outgoing Y system.

2 Data selection and kinematics

2.1 Event selection

The data used for the present analysis were taken with the H1 detector in the year 2000. The energies of the HERA proton and positron beams [1] were 920 and 27.5 GeV, respectively. The integrated luminosity used for the analysis amounts to 42.4 pb^{-1}.

The relevant parts of the detector, for which more details can be found in [2, 6], are the central tracking detector, the liquid argon (LAr) and the backward electromagnetic (SPACAL) calorimeters and the forward detectors, which are sensitive to energy flow close to the outgoing proton direction [2]: the proton remnant tagger (PRT), a set of 7 scintillator layers surrounding the beam pipe 24 m downstream of the ep interaction point, and the three planes of the forward muon detector (FMD) situated between the interaction point and the solenoidal magnet.

Events corresponding to reaction (1), in the kinematic range defined by relations (2) are selected by requesting :

[1] In the following, the word electron will be used for both electrons and positrons.

[2] In the H1 convention, the z axis is defined by the colliding beams, the forward direction being that of the outgoing proton beam ($z > 0$) and the backward direction that of the electron beam ($z < 0$).

- the reconstruction of a cluster in the SPACAL calorimeter with energy larger than 17 GeV (the scattered electron candidate)

- the reconstruction in the central tracking detector of the trajectories of exactly two charged particles (pion candidates) with opposite charges, transverse momenta larger than 0.1 GeV and polar angles confined within the interval $20^o < \theta < 160^o$.

- the invariant mass $M_{\pi\pi}$ of the decay pions to be restricted to $0.6 < M_{\pi\pi} < 1.1 GeV$.

- the absence of any energy deposit larger than 400 MeV in the LAr calorimeter, which is not associated with the electron or the two charged pion candidates. This cut reduces backgrounds due to the diffractive production of systems decaying into two charged and additional neutral particles. It also helps rejecting proton dissociative events with large M_Y masses.

- the absence of activity above noise in the PRT and the FMD, in order to reject events with proton dissociation.

- events with $M_{KK} < 1.04$ GeV are discarded, where M_{KK} is the invariant mass of the two hadron candidates when considered as kaons (no direct hadron identification is performed for this analysis). This cut reduces the background due to diffractive production of ϕ mesons.

- a cut $\sum(E - p_z) > 45$ GeV is applied, in order to reduce QED radiative corrections. $\sum(E - p_z)$ is the difference of the energies and the longitudinal momenta of the scattered electron (measured in the SPACAL) and the pion candidates (measured in the central tracking detector); it is expected to be close to twice the incident electron beam energy, i.e. 55 GeV, if no other particles have been produced except for the forward going system Y, in particular high energy photons radiated by the electron.

To first approximation, the selected events can be attributed to elastic scattering.

2.2 Monte Carlo simulations

A Monte Carlo simulation based on the DIFFVM program [8] including QED radiation [9] is used to describe the elastic production and decay of ρ vector mesons, and to correct the data for acceptance, smearing and radiative effects.

The DIFFVM simulation is also used for the description of the ρ proton dissociative, ω, ϕ and ρ' backgrounds.

3 Cross sections

In each bin of the kinematical variables, the cross section is computed from the numbers of events in the bin, fully corrected for backgrounds, acceptance, smearing and radiation effects using the Monte Carlo simulations described above. It is converted into a $\gamma^* p$ cross section using the relation:

$$\frac{d^2\sigma_{tot}(ep \to e\rho p)}{dy\, dQ^2} = \Gamma\, \sigma_{tot}(\gamma^* p \to Vp) = \; \Gamma\, \sigma_T(\gamma^* p \to \rho p)\; (1 + \varepsilon\, R), \tag{3}$$

where σ_{tot}, σ_T and σ_L are the total, transverse and longitudinal $\gamma^* p$ cross sections,

$$R\; = \sigma_L/\sigma_T, \tag{4}$$

and Γ is the flux of transverse virtual photons given by

$$\Gamma = \frac{\alpha_{em}\; (1 - y + y^2/2)}{\pi\; yQ^2}; \tag{5}$$

ε is the polarisation parameter

$$\varepsilon = \frac{1 - y}{1 - y + y^2/2}. \tag{6}$$

For this experiment, $\varepsilon = 0.996$. The Q^2 and W dependences used for the computation of the flux factors were taken from the present analysis.

The mass distributions were corrected for the analysis cut, to the range ($2m_\pi < m_{\pi\pi} < m_\rho + 5\Gamma_\rho$), where m_π and m_ρ are the pion and ρ meson masses, respectively.

3.1 Q^2 dependence of the $\gamma^* p$ cross section

Fig. 1 presents the Q^2 dependence of the $\gamma^* p$ cross section, for $W = 95$ GeV. A fit of the form $\mathrm{d}\sigma/\mathrm{d}Q^2 \propto 1/(Q^2 + m_\rho^2)$ for the range $8 < Q^2 < 60$ GeV^2 results in $n = 2.60 \pm 0.04$, with $\chi^2/ndf = 4.6/10$.

3.2 W dependence of the $\gamma^* p$ cross section

Fig. 2 presents the W dependence of the $\gamma^* p$ cross section, for four bins in Q^2. The cross section rise with W is observed to be stronger as Q^2 increases. The W dependence at fixed Q^2 being parameterised as $\mathrm{d}\sigma/\mathrm{d}W \propto W^\delta$, the fitted values of δ are shown in Fig. 3, together with previous measurements. Values of order 1. are reached for the highest Q^2 range, similar to measurements for J/ψ photoproduction [16].

3.3 t dependence of the ep cross section

The $|t|$ dependence of the $e + p \to e + \rho + p$ cross section has been extracted for four intervals in Q^2. The slopes resulting from exponential fits to the data are shown as a function of Q^2 in fig. 4, together with previous measurements. As Q^2 increases, they decrease down to values close to those obtained for J/ψ photoproduction are obtained [16].

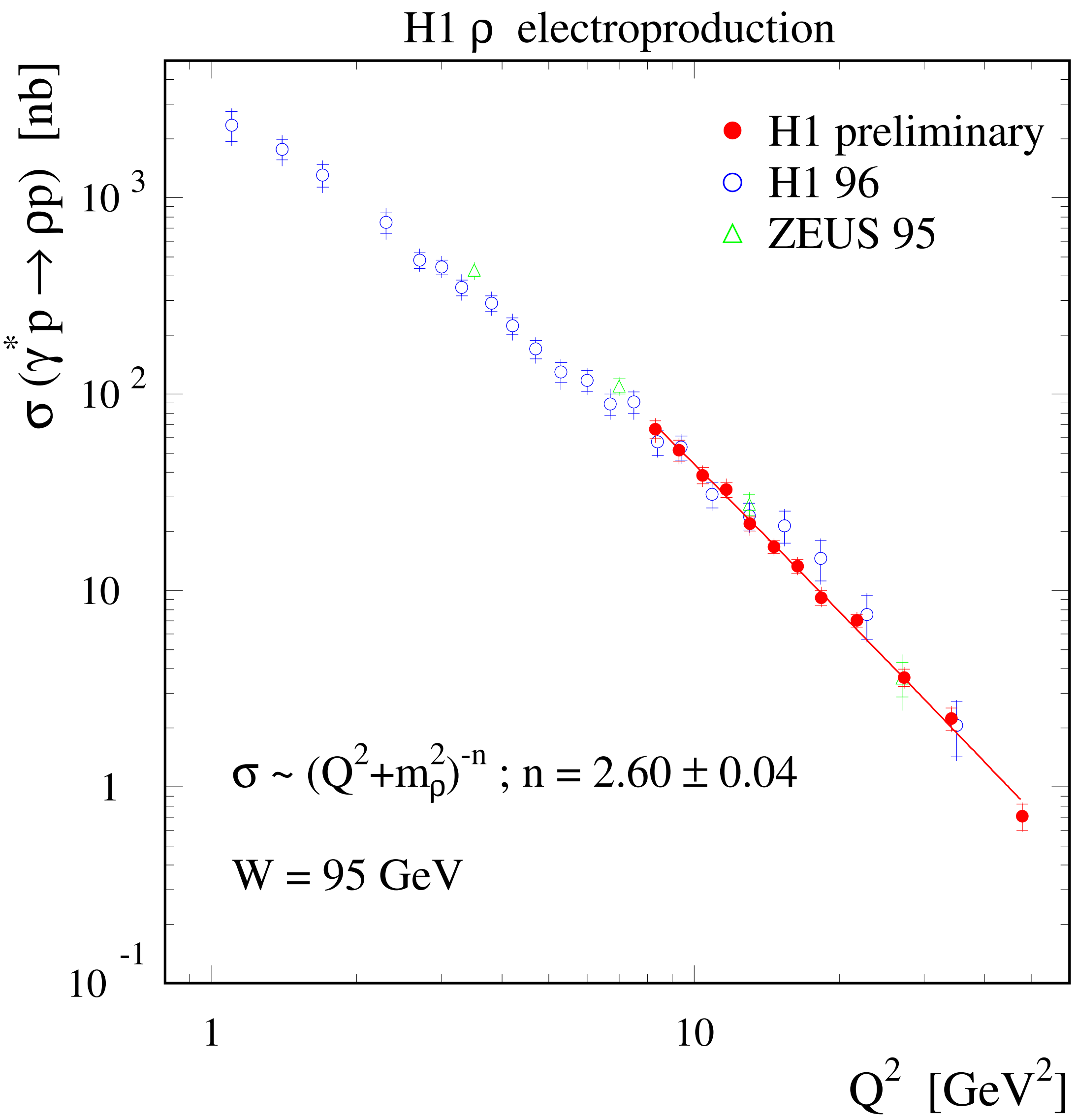

Figure 1: The $\gamma^* p \to \rho + p$ cross section as a function of Q^2, for $W = 95$ GeV. Also shown are the data [2], extrapolated to same W value using the W dependences measured in the present analysis. The inner error bars are statistical, and the full error bars include the systematic errors added in quadrature. The superimposed line is for $\mathrm{d}\sigma/\mathrm{d}Q^2 \propto 1/(Q^2 + m_\rho^2)$ with $n = 2.60$. The fit error include both statistical and uncorrelated systematic errors.

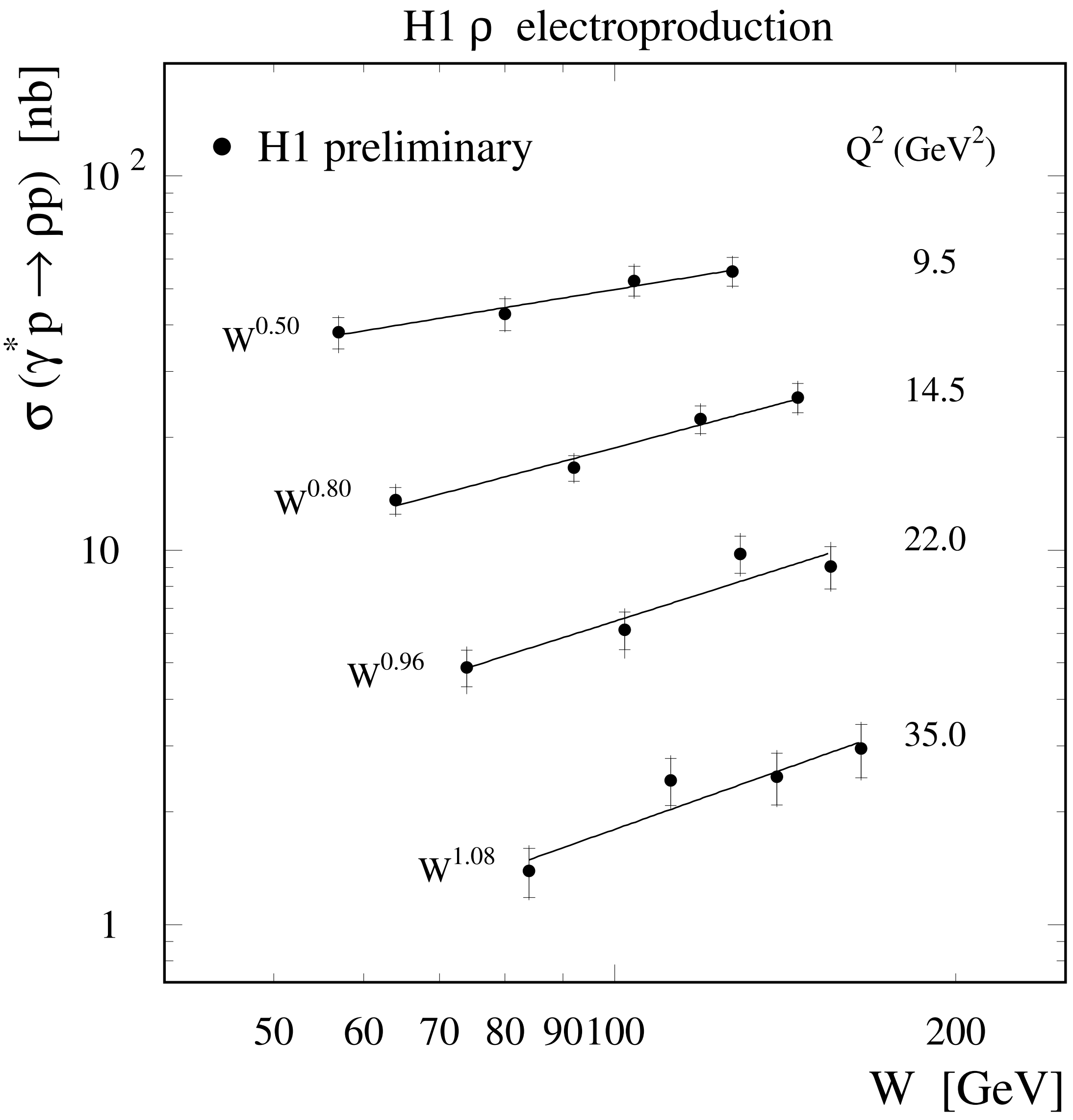

Figure 2: The $\gamma^* p \rightarrow \rho + p$ cross section as a function of W for several Q^2 values. The inner error bars are statistical, and the full error bars include the systematic errors added in quadrature. The superimposed line represents parameterisations of the form $\mathrm{d}\sigma/\mathrm{d}W \propto W^{\delta}$.

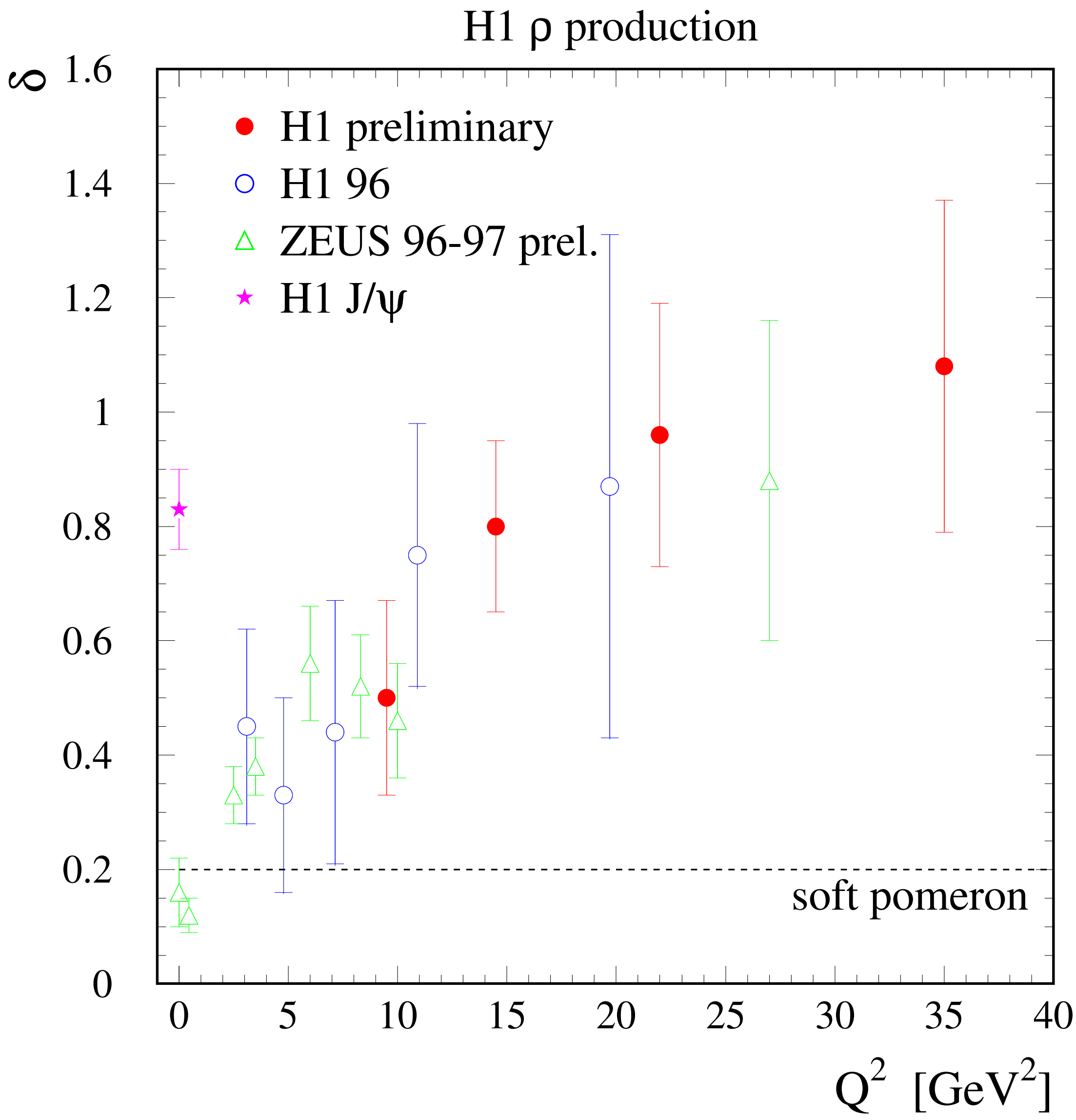

Figure 3: Results of fits of the form $\mathrm{d}\sigma/\mathrm{d}W \propto W^{\delta}$ to the W dependence of the $\gamma^{*}p$ cross section, presented as a function of Q^2. Also shown are the measurements [2] and [15] for ρ meson production and [16] for J/ψ photoproduction. The errors include both statistical and uncorrelated systematic errors.

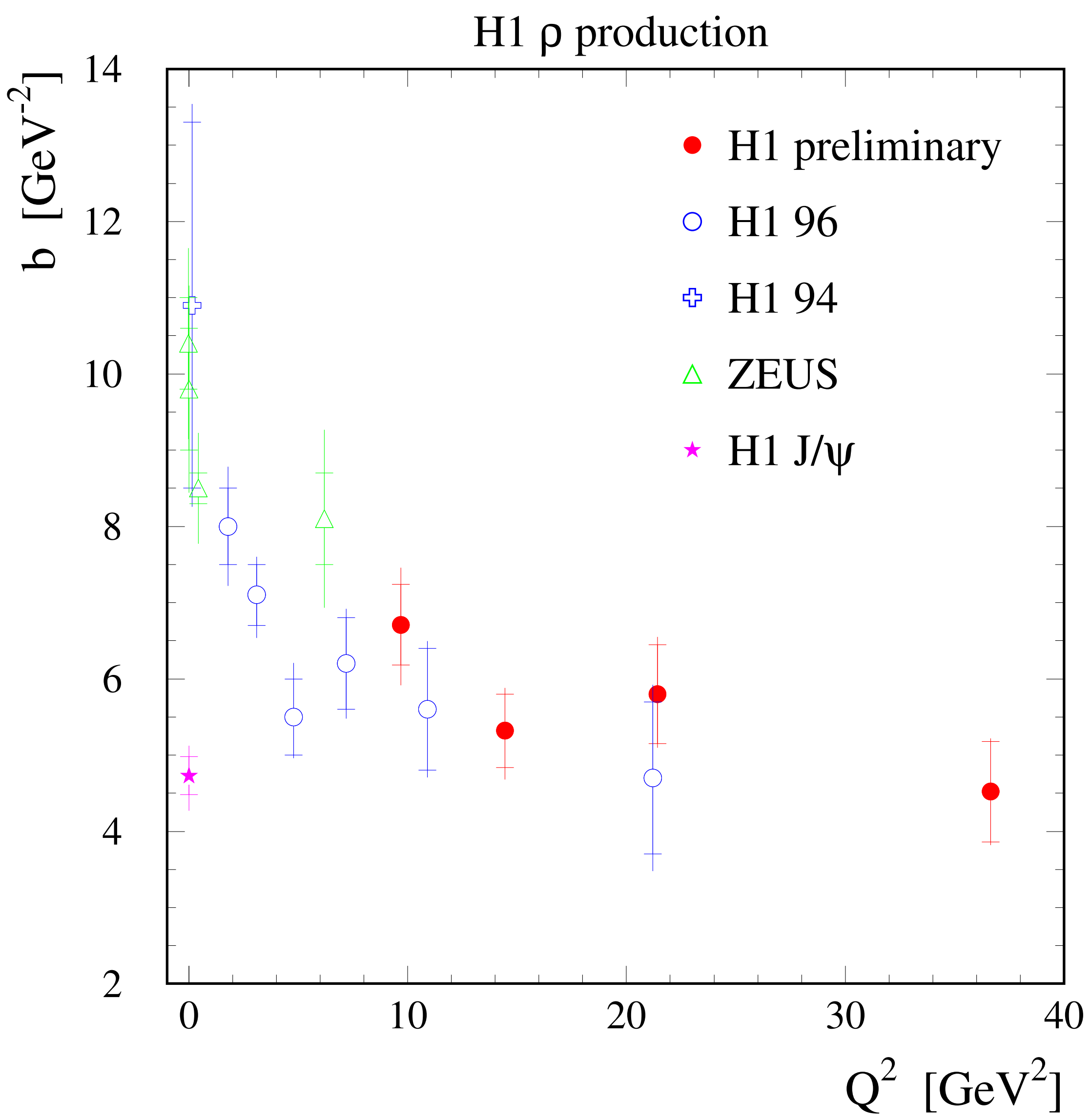

Figure 4: Results of fits to exponential distributions of the to the $|t|$ dependence of the $e+p \rightarrow e+\rho+p$ cross section, presented as a function of Q^2. Also shown are the measurements [2], [17] and [15] for ρ meson production and [16] for J/ψ photoproduction. The inner error bars are statistical, and the full error bars include the systematic errors added in quadrature.

3.4 r^{04}_{00} spin density matrix element

The $\cos\theta^*$ dependence of the $e + p \to e + \rho + p$ cross section, for three intervals in Q^2, three intervals in W and three intervals in $|t|$have been fitted to the form

$$\frac{\mathrm{d}\sigma}{\mathrm{d}\cos\theta^*} \propto 1 - r^{04}_{00} + (3\, r^{04}_{00} - 1)\cos^2\theta^*. \tag{7}$$

The extracted values of the r^{04}_{00} spin density matrix element are shown as a function of Q^2, W and $|t|$ in fig. 5. Fig. 7 presents the corresponding value of $R = \sigma_L/\sigma_T$, extracted under the s-channel helicity conservation approximation, together with previous measurements.

The r^{04}_{00} matrix element increases with Q^2, indicating a significant increase of the longitudinal to transverse cross section ratio, up to the highest available Q^2 values. In contrast, r^{04}_{00} is independent of W and $|t|$, the latter feature indicating that, in the measured range, the longitudinal and transverse $|t|$ distributions have the same behaviour.

3.5 $(r^5_{00} + 2r^5_{11})$ and $(r^1_{00} + 2r^1_{11})$ combinations

The Φ dependence of the $e + p \to e + \rho + p$ cross section, for three intervals in Q^2, three intervals in W and three intervals in $|t|$have been fitted to the form

$$\frac{\mathrm{d}\sigma}{\mathrm{d}\Phi} \propto 1 + \sqrt{2\epsilon(1+\epsilon)}\ \cos\Phi\ (r^5_{00} + 2r^5_{11}) - \epsilon\ \cos 2\Phi\ (r^1_{00} + 2r^1_{11}) \tag{8}$$

The extracted combinations of spin density matrix elements $r^5_{00} + 2r^5_{11}$ and $r^1_{00} + 2r^1_{11}$ are shown as a function of Q^2, W and $|t|$ in figs. 8 and 10, respectively.

Values significantly different of 0 and increasing with $|t|$ are obtained for the $r^5_{00} + 2r^5_{11}$ combination, confirming s-channel helicity non conservation [2, 3, 19].

4 Conclusions

The elastic electroproduction of ρ mesons, $e + p \to e + \rho + p$, has been studied at HERA in the kinematic range $8 < Q^2 < 60$ GeV^2, $40 < W < 180$ GeV, $0 < |t| < 0.5$ GeV^2.

The Q^2, W and t dependences of the $\gamma^* p$ cross section have been measured. The Q^2 distribution is well described in the form $\mathrm{d}\sigma/\mathrm{d}Q^2 \propto 1/(Q^2 + m^2_\rho)$, with $n = 2.60 \pm 0.04$. The W dependence at fixed Q^2 of the cross section, when parameterised as $\mathrm{d}\sigma/\mathrm{d}W \propto W^\delta$, indicates a significant increase of the fitted values of δ with Q^2, reaching for the highest Q^2 interval values of order 1., similar to J/ψ photoproduction measurements. Fits to exponential distributions of the $|t|$ dependence of the cross section give slopes decreasing with increasing Q^2, reaching for the highest Q^2 data values close to those obtained for J/ψ photoproduction.

The r^{04}_{00} spin density matrix element and the combinations $r^5_{00} + 2r^5_{11}$ and $r^1_{00} + 2r^1_{11}$ have been measured as a function of Q^2, W and $|t|$. The r^{04}_{00} matrix element increases with Q^2, indicating a significant increase of the longitudinal to transverse cross section ratio, up to the highest available Q^2 values. In contrast, r^{04}_{00} is independent of W and $|t|$, the latter feature indicating that, in the measured range, the longitudinal and transverse $|t|$ distributions have the same behaviour. Values significantly different of 0 and increasing with $|t|$ are obtained for the $r^5_{00} + 2r^5_{11}$ combination, confirming s-channel helicity non conservation [2, 3, 19].

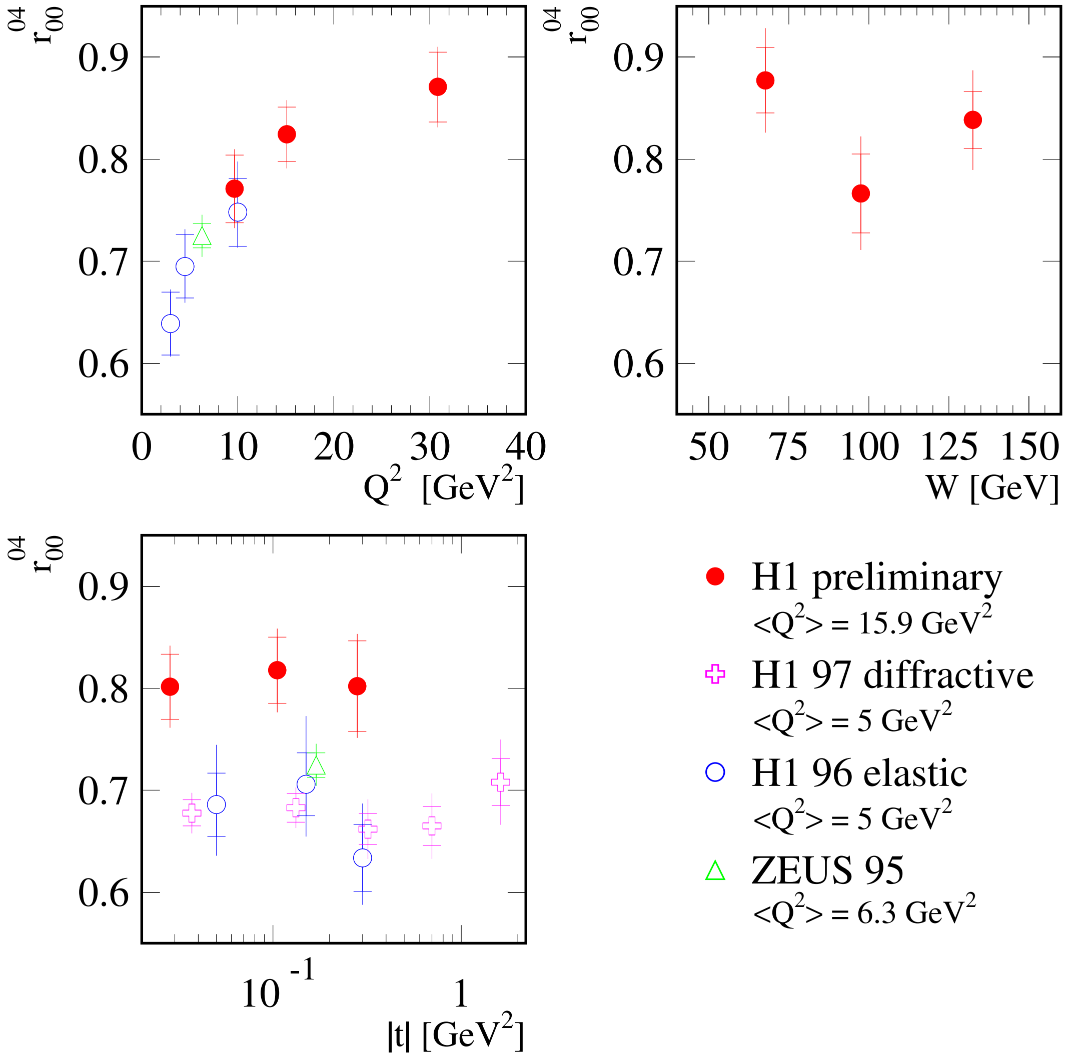

Figure 5: Measurments of r_{00}^{04}as a function of Q^2, W and $|t|$. Also shown are measurments [2,3,19]. The inner error bars are statistical, and the full error bars include the systematic errors added in quadrature.

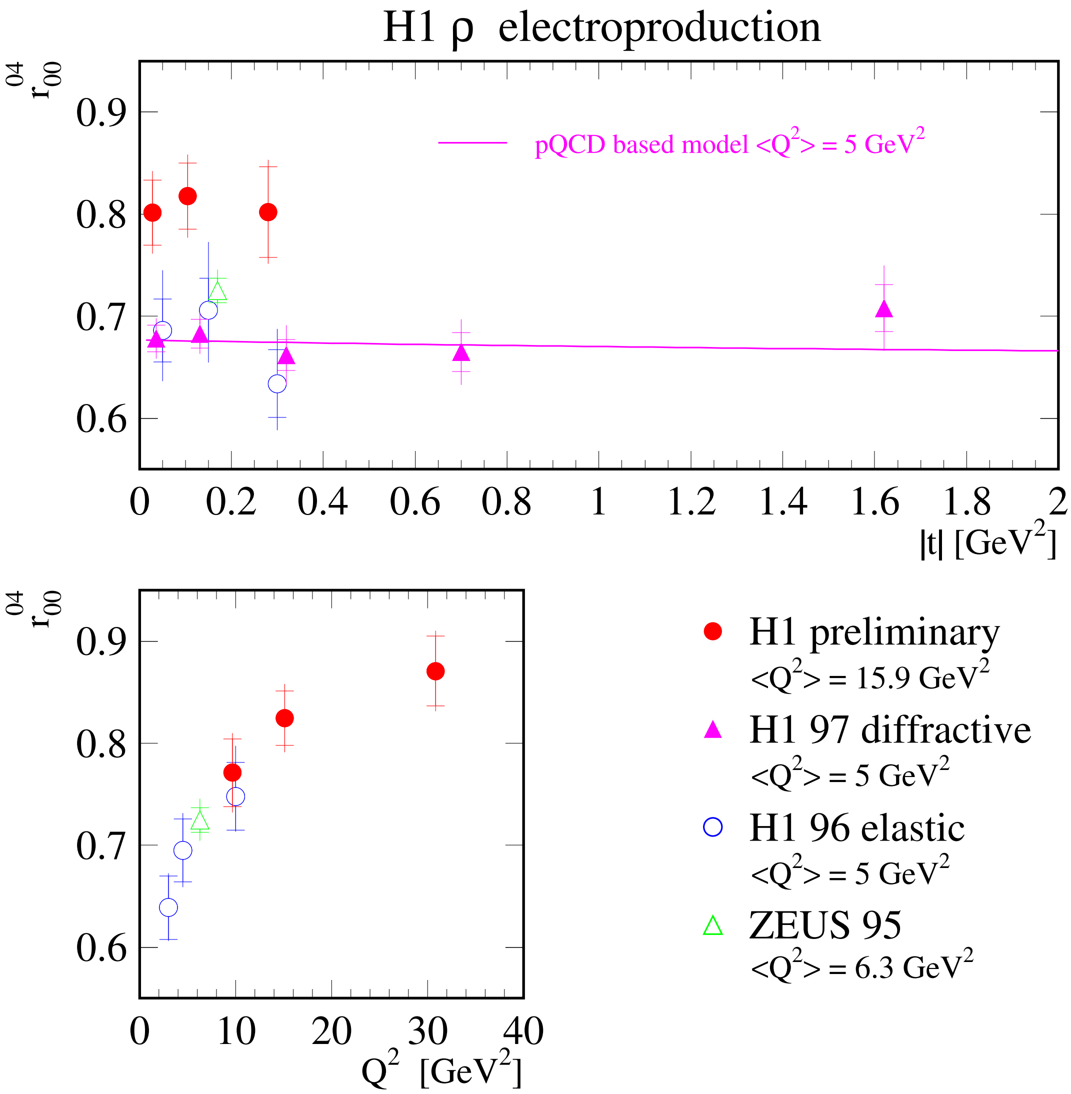

Figure 6: Same as figure 5 on different scales.

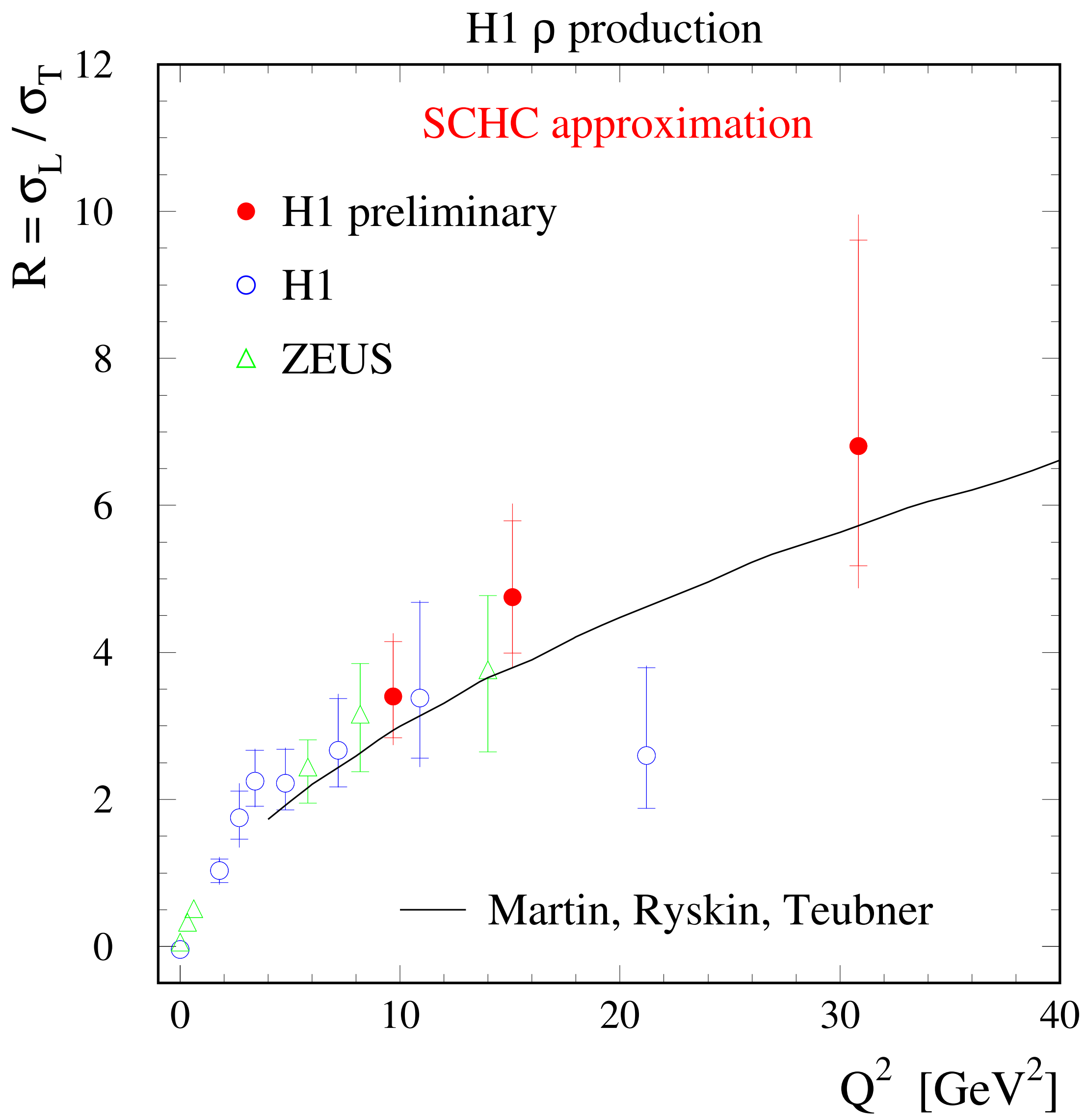

Figure 7: The ratio R of cross sections for elastic ρ meson electroproduction by longitudinal and transverse photons, measured in the SCHC approximation and presented as a function of Q^2. The other measurements are from H1 [2, 17] and ZEUS [15, 18]. The inner error bars are statistical, and the full error bars include the systematic errors added in quadrature.

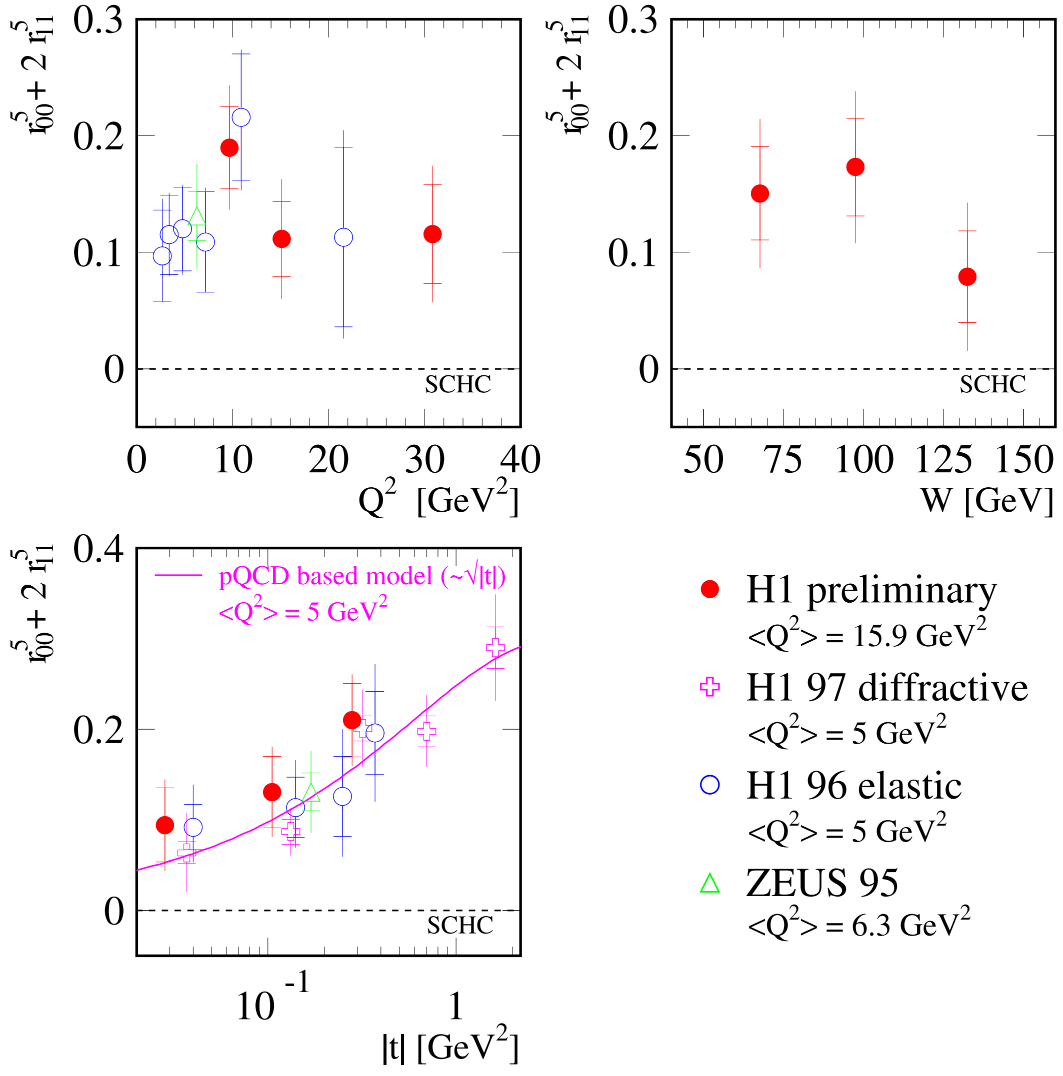

Figure 8: Measurments of $r^5_{00} + 2r^5_{11}$as a function of Q^2, W and $|t|$. Also shown are measurments [2, 3, 19]. The superimposed line is taken from [3]. The inner error bars are statistical, and the full error bars include the systematic errors added in quadrature.

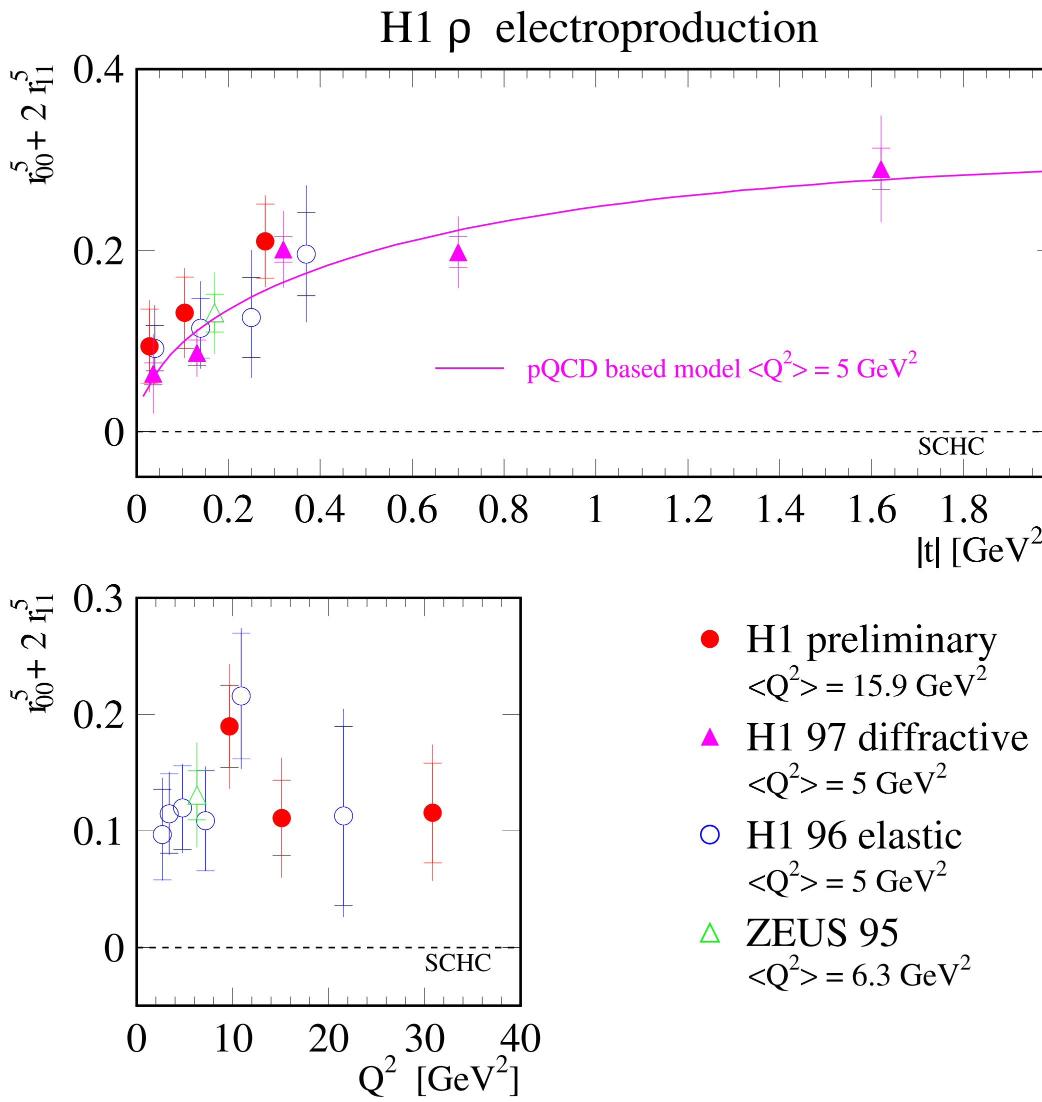

Figure 9: Same as figure 8 on different scales.

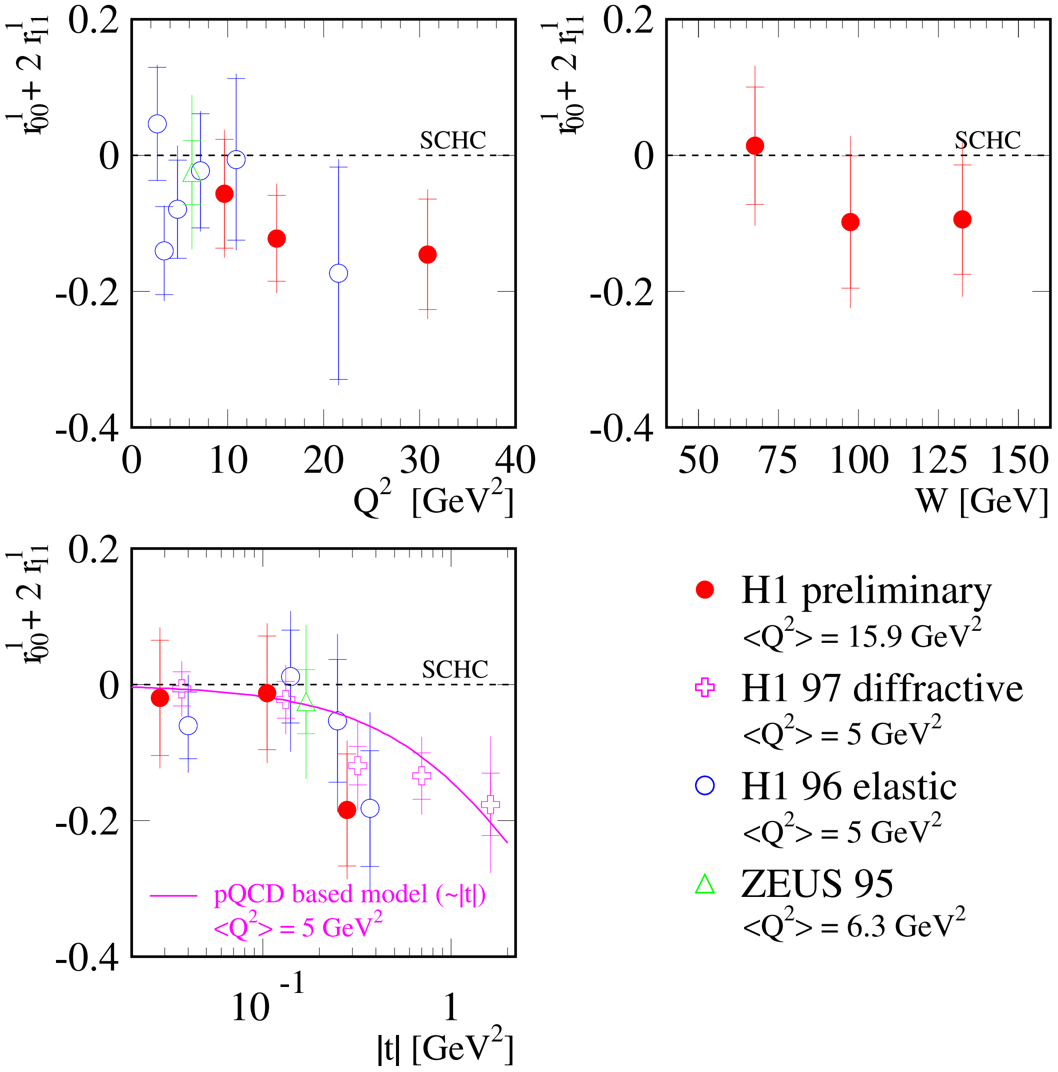

Figure 10: Measurments of $r^1_{00} + 2r^1_{11}$as a function of Q^2, W and $|t|$. Also shown are measurments [2, 3, 19]. The superimposed line is taken from [3]. The inner error bars are statistical, and the full error bars include the systematic errors added in quadrature.

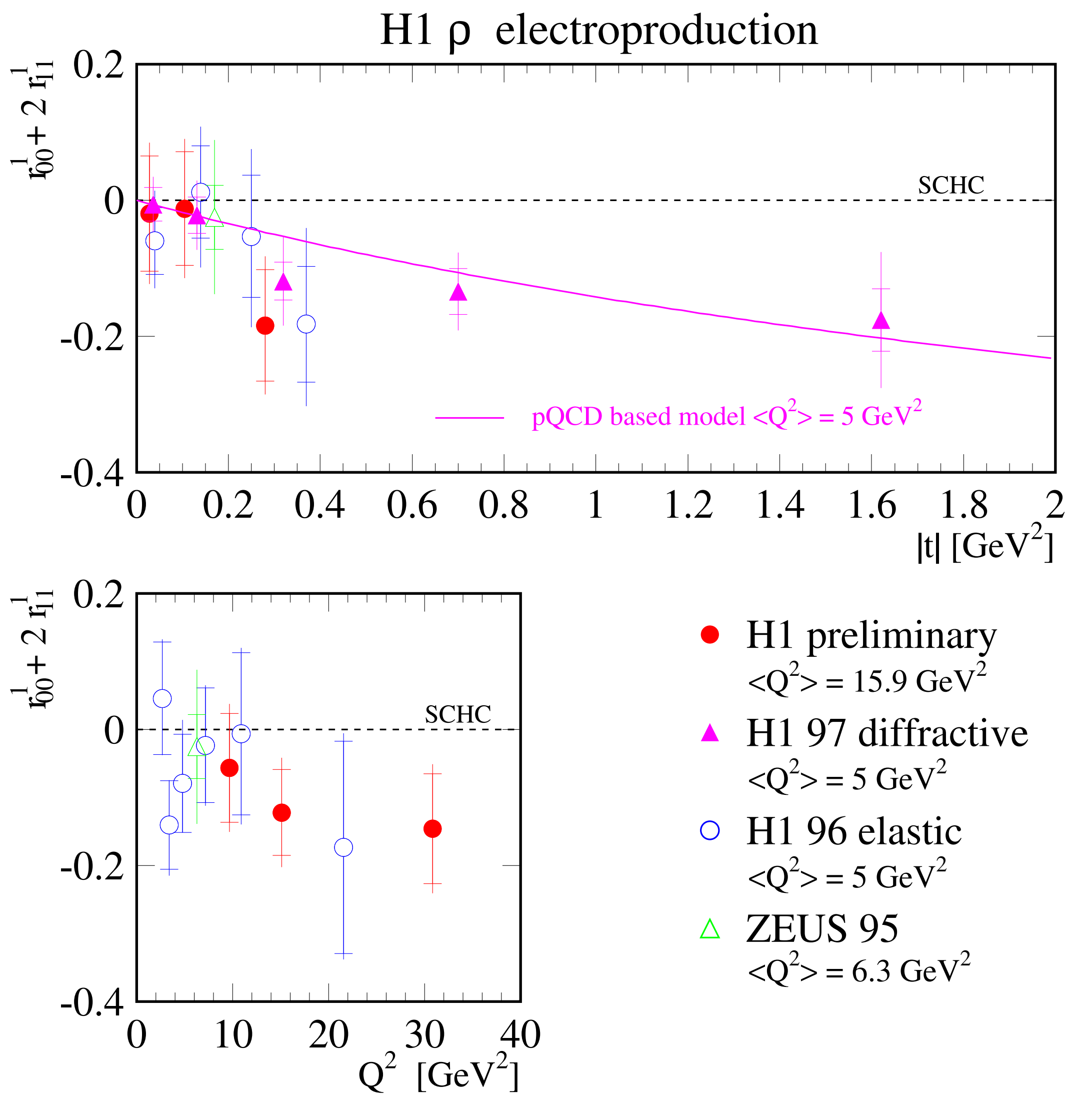

Figure 11: Same as fig 10 on different scales.

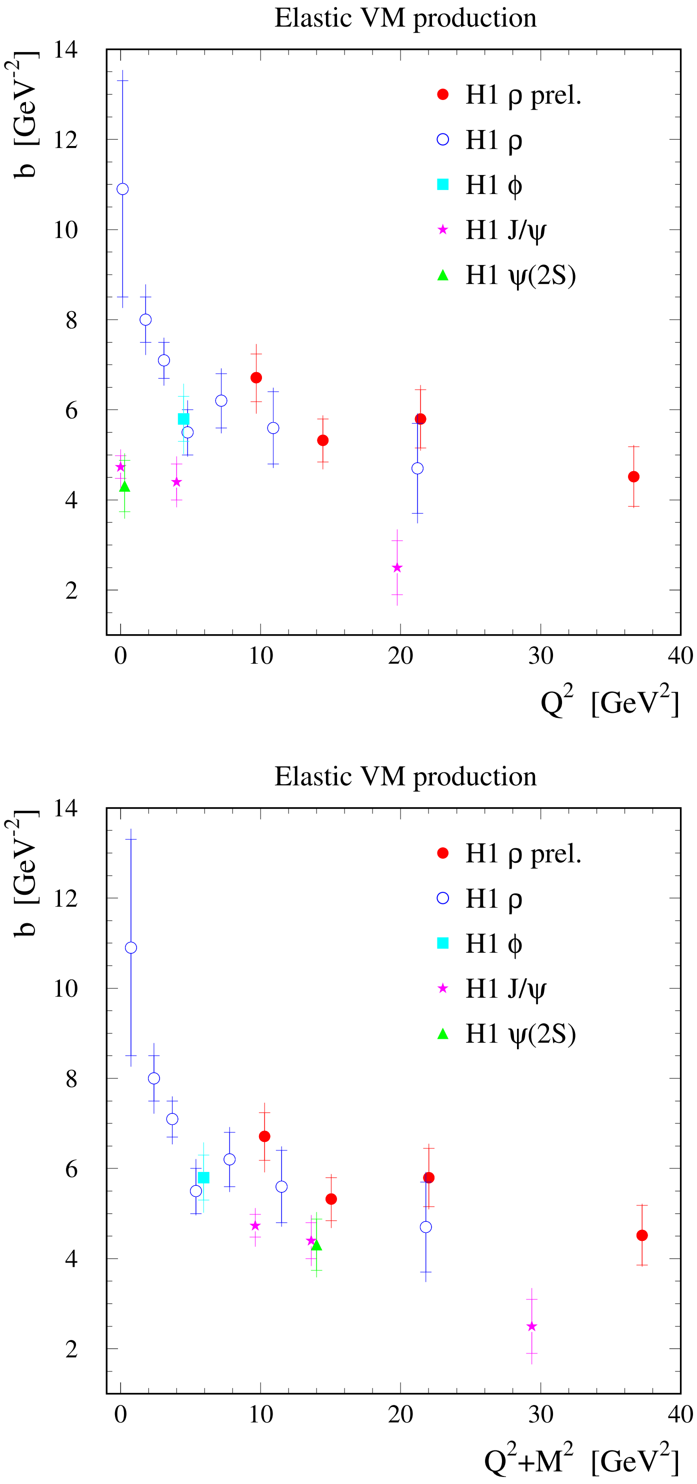

Figure 12: b slope as function of Q^2 and $Q^2 + M^2$.

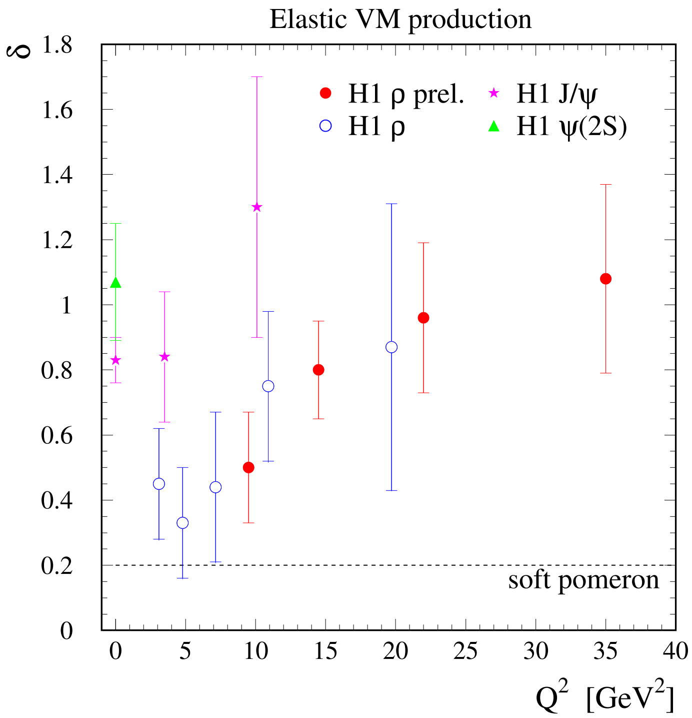

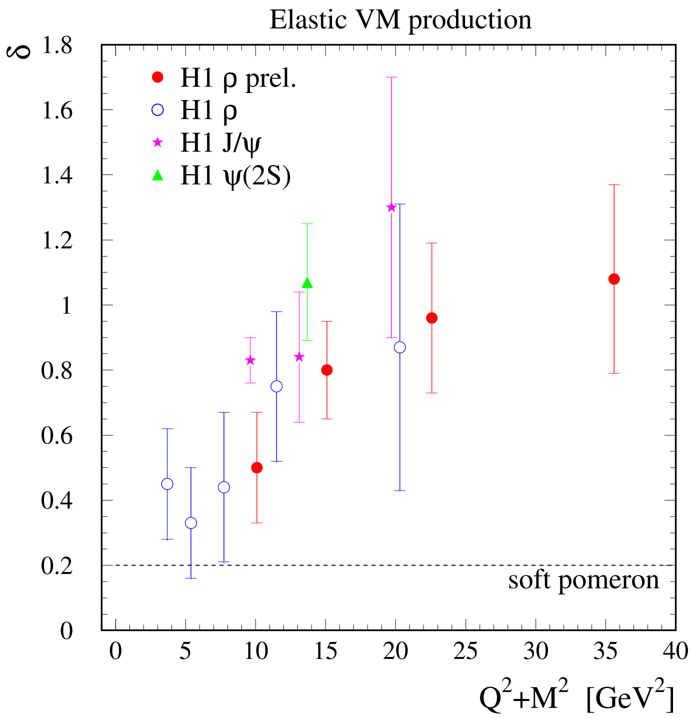

Figure 13: δ as function of Q^2 and $Q^2 + M^2$.

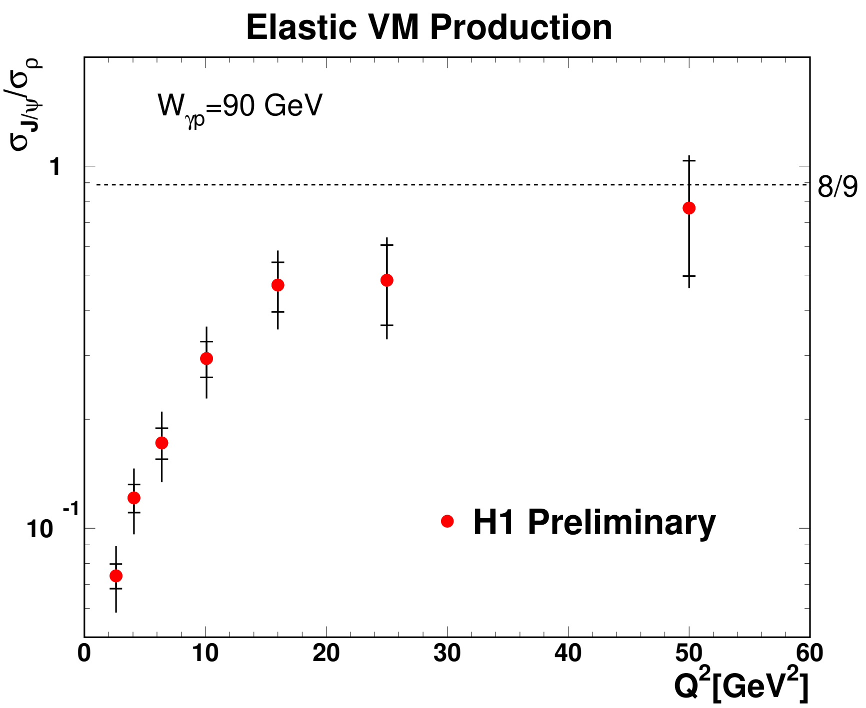

Figure 14: Cross section ratio for ρ and J/Ψ.

Acknowledgements

We are grateful to the HERA machine group whose outstanding efforts have made and continue to make this experiment possible. We thank the engineers and technicians for their work in constructing and now maintaining the H1 detector, our funding agencies for financial support, the DESY technical staff for continual assistance, and the DESY directorate for the hospitality which they extend to the non DESY members of the collaboration.

References

[1] K. Schilling and G. Wolf, Nucl. Phys. **B61** (1973) 381.

[2] C. Adloff *et al.* [H1 Collaboration], Eur. Phys. J. **C13** (2000) 371 [hep-ex/9902019].

[3] C. Adloff *et al.* [H1 Collaboration], " A measurement of the t dependence of the helicity structure of diffractive ρ meson electroproduction at HERA", subm. to Phys. Lett. [hep-ex/0203022].

[4] J. Breitweg *et al.* [ZEUS Collaboration], Eur. Phys. J. **C12** (2000) 393 [hep-ex/9908026]; J. Breitweg *et al.* [ZEUS Collaboration], Eur. Phys. J. **C6** (1999) 603 [hep-ex/9808020].

[5] C. Adloff *et al.* [H1 Collaboration], Phys. Lett. **B483** (2000) 360 [hep-ex/0005010].

[6] I. Abt *et al.* [H1 Collaboration], Nucl. Instr. Meth. **A386** (1997) 310 and 348;
R. D. Appuhn *et al.* [H1 SPACAL Group], Nucl. Instr. Meth. **A386** (1997) 397.

[7] S. Bentvelsen, J. Engelen and P. Kooijman, in Proc. of the Workshop on Physics at HERA, W. Buchmüller and G. Ingelman ed., Hamburg (1992) 23; K.C. Hoeger, ibid, p 43.

[8] B. List and A. Mastroberardino, in Proc. of the Workshop on Monte Carlo Generators for HERA Physics, A.T. Doyle et al. ed., DESY-PROC-1999-02 (1999) 396.

[9] A. Kwiatkowski, H.-J. Möhring and H. Spiesberger, Comput. Phys. Commun. **69** (1992), 155 and Proc. of the Workshop on Physics at HERA, W. Buchmüller and G. Ingelman ed., Hamburg (1992) 1294.

[10] C. Adloff *et al.* [H1 Collaboration], Z. Phys. **C75** (1997) 607 [hep-ex/9705014].

[11] K. Goulianos, Phys. Rep. **101** (1983) 169.

[12] J. Breitweg *et al.* [ZEUS Collaboration], Phys. Lett. **B487** (2000) 273 [hep-ex/0006013].

[13] Review of Particle Physics [Part. Data Group], Eur. Phys. J. **C15** (2000) 1.

[14] M. Ross and L. Stodolsky, Phys. Rev. **149** (1966) 1173.

[15] ZEUS Collaboration, "Exclusive electroproduction of ρ^0 mesons at HERA", Contrib. pap. 594 to the Eur. Phys. Soc. Conference, Budapest 2001.

[16] C. Adloff *et al.* [H1 Collaboration], Phys. Lett. **B483** (2000) 23

[17] S. Aid *et al.* [H1 Collaboration], Nucl. Phys. **B463** (1996) 3

[18] J. Breitweg *et al.*, [ZEUS Collaboration], Eur. Phys. J. **C2** (1998) 247

[19] J.Breitweg *et al* [ZEUS Collaboration], Eur. Phys. J. **C14** (2000) 213.:q